Supplementary Information

Human Antibody-Based Chemically Induced Dimerizers for Cell Therapeutic Applications

Zachary B Hill[1,4], Alexander J Martinko[1,2,4], Duy P Nguyen[1] & James A Wells[*1,3]

[1]Department of Pharmaceutical Chemistry, University of California, San Francisco, California, USA. [2]Chemistry and Chemical Biology Graduate Program, University of California, San Francisco, California, USA. [3]Department of Cellular and Molecular Pharmacology, University of California, San Francisco, California, USA. [4]These authors contributed equally to this work. Correspondence should be addressed to J.A.W. (jim.wells@ucsf.edu)

Supplementary Results

Fab ID	CDR L3	CDR H1	CDR H2	CDR H3
AZ1	YYWGFPSLF	LSYSSM	SISPYSSYTS	GWVGM
AZ2	VSWAYPYLI	IYSYYM	YISPYYSYTS	GYPWYGM
AZ3	GWSGPWLI	IYYSYM	SISPYSSYTS	YGYSYYYYGAL
AZ4	VPAFPI	IYSSSI	SIYPYYGYTY	SWWPYGM
AZ5	WPGWYPI	LYYYYI	SIYPSYGSTY	ASVWFGWYVPSAM
AZ6	SSYSLI	LSYSYI	SIYSSSGSTY	GSHAHGWAWFWYGM
AZ7	SSYSLI	LSSYSM	SIYSYYGSTS	YSPWVYYPYYGWYSGM
AZ8	SGWFFPF	ISYSSI	SISSYYGSTS	TVRGSKKPYFSGWAM
AZ9	SYYYYSGPI	LYYSSI	SISSSYGYTY	TVRGSKKPYFSGWAM
AZ10	SYYFYSGPI	LYSYSM	SISSYYSSTY	TVRGSKKPYFSGWAM

Supplementary Table 1 Sequences of chemically inducible BCL-xL binding Fab clones. Shown are the amino acid sequences of the complementarity determining regions (CDRs) of all unique Fab clones presented in this study.

Fab ID	ABT-737 1μM	K_D (10^{-9}M)	k_{ON} ($10^5 M^{-1}s^{-1}$)	k_{OFF} ($10^{-4}s^{-1}$)
AZ1	+	3.0	1.3	4.0
	-	>5000	N.D.	N.D.
AZ2	+	2.4	1.1	2.6
	-	>5000	N.D.	N.D.
AZ3	+	9.5	2.2	20.9
	-	>5000	N.D.	N.D.

Supplementary Table 2 Binding and kinetic constants measured for binding of Fabs AZ1–AZ3 to BCL-xL in the presence or absence of ABT-737. N.D. indicates the values could not be determined due to absence of detectable binding.

Protein ID	T_m (˚C) (0.05% DMSO)	T_m (˚C) (20μM ABT-737)	ΔT_m (˚C)
AZ1	78.6	79.0	0.4
AZ2	84.1	84.5	0.4
AZ3	78.4	78.7	0.3
AZ4	80.5	80.5	0.0
AZ5	78.1	78.3	0.2
AZ6	79.6	79.6	0.0
AZ7	75.1	75.3	0.2
AZ8	76.1	76.5	0.4
AZ9	78.2	78.5	0.3
AZ10	76.3	77.0	0.7
Isotype Control	85.0	85.3	0.3
BCL-xL	76.7	86.9	10.2

Supplementary Table 3 Differential Scanning Fluorimetry of Fabs and BCL-xL in the presence of ABT-737. Fabs AZ1–AZ10 show no significant T_m shift in the presence of ABT-737, supporting that they do not bind ABT-737 in the absence of BCL-xL. In comparison, BCL-xL, which is know to potently bind ABT-737, shows a 10 °C increase in T_m in the presence of ABT-737. The isotype control is a Fab selected against eGFP, with an identical scaffold to AZ1 but differing CDR sequences. Each data point represents the mean of 3 independent experiments. Instrument measurement co-variation was determined to be ± 0.29 °C.

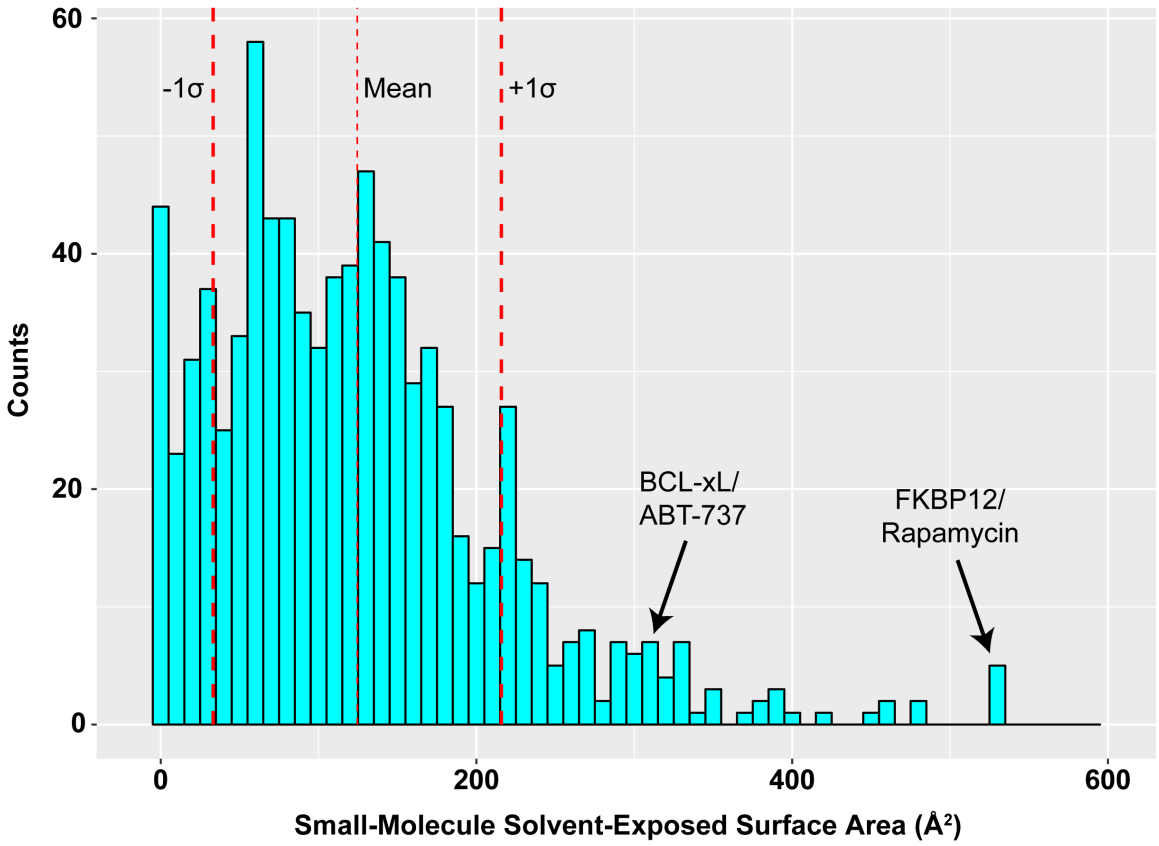

Supplementary Figure 1 Analysis of the solvent accessibility of the small molecule in 866 small-molecule-protein complex crystal structures from the Protein Data Bank. We hypothesized that the large amount of solvent-exposed surface area of ABT-737 when in complex with BCL-xL (308 $Å^2$) would provide a chemical epitope for direct recognition by an antibody. The FKBP12/rapamycin complex (528 $Å^2$), which is part of a naturally occurring CID, is a stark outlier in this analysis, supporting our hypothesis.

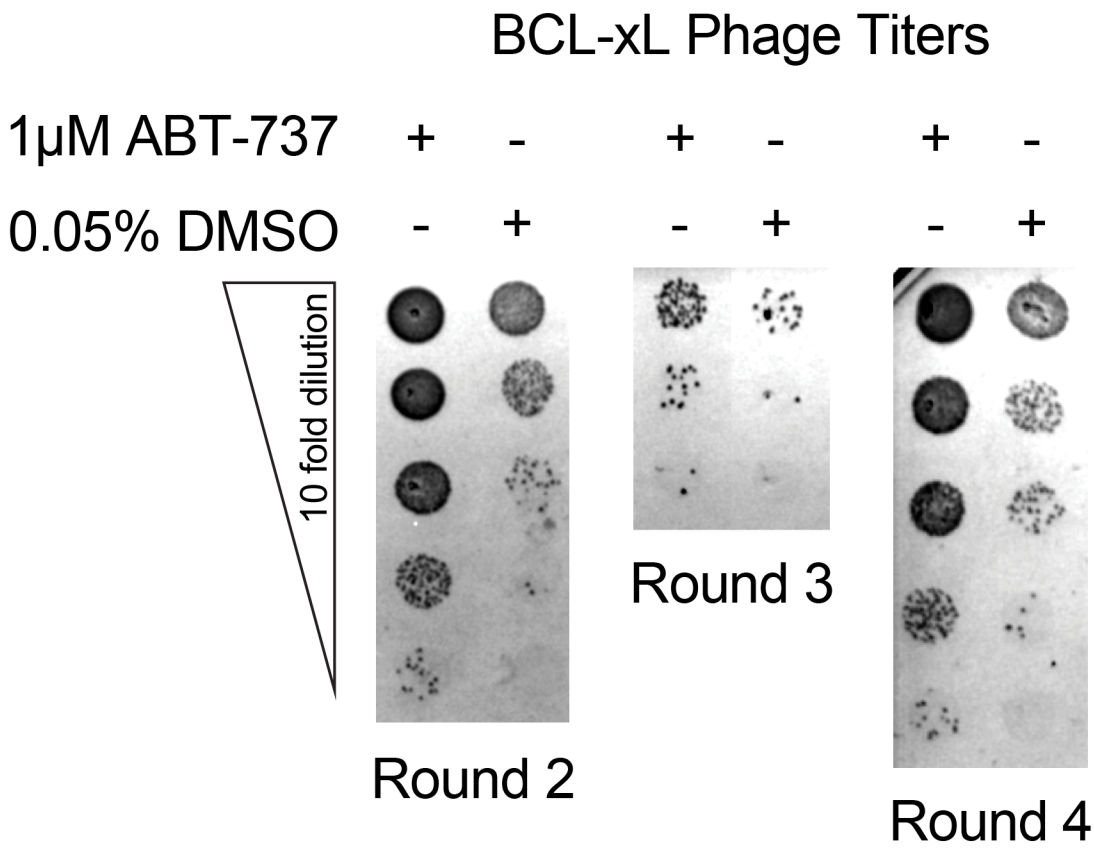

Supplementary Figure 2 Representative titers of phage libraries from Rounds 2 through 4 of Fab-phage selections against BCL-xL bound to ABT-737. Greater than ten-fold enrichment of phage was observed for binding of BCL-xL in the presence of 1 μM ABT-737 compared to DMSO as determined by quantification of recovered colony forming units.

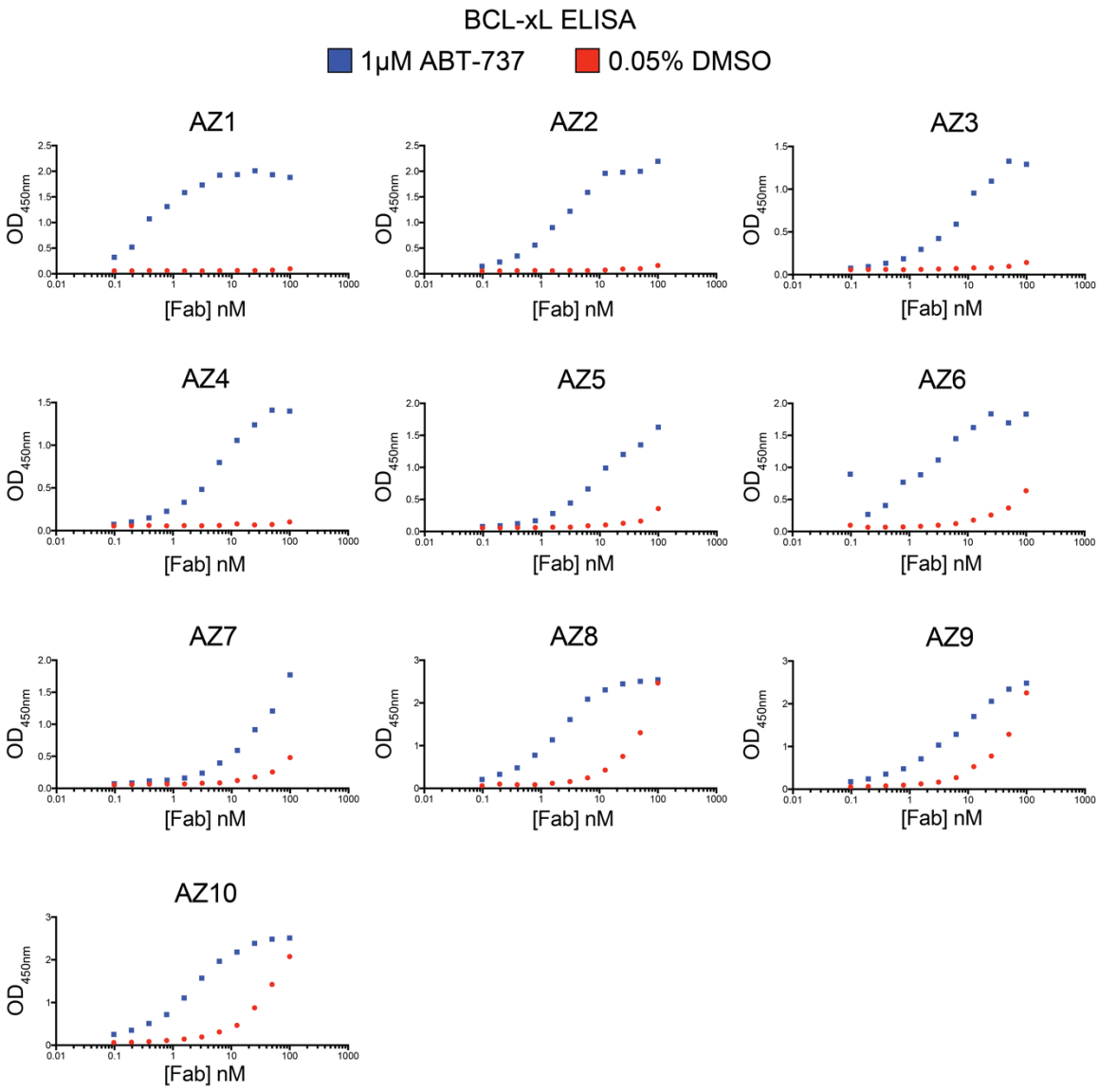

Supplementary Figure 3 ELISA of purified sequence-unique Fabs derived from ABT-737-bound BCL-xL selections. All Fabs showed enhanced binding in the presence of ABT-737. Four out of the ten Fabs tested (AZ 1–4) exhibited high potency and dose-dependent binding to BCL-xL in the presence of ABT-737 with virtually no appreciable binding in the absence of ABT-737. Each data point represents a single measurement.

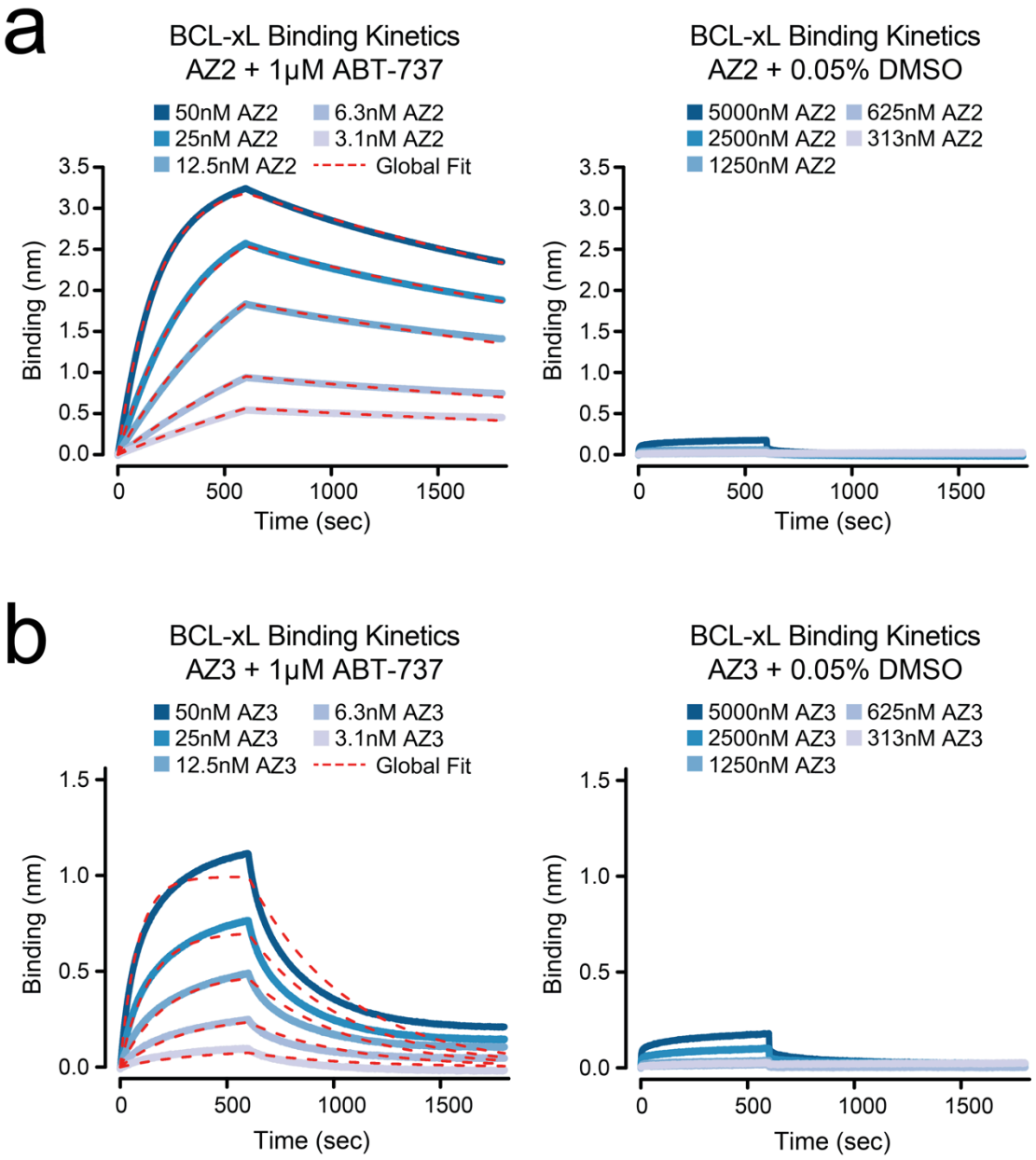

Supplementary Figure 4 Biolayer interferometry of Fabs AZ2 and AZ3. Blue curves represent measured data points and dashed red lines represent the global-fit lines used for analysis **(a)** Fab AZ2 shows potent and reversible binding to BCL-xL in the presence of ABT-737 (left) and no significant binding was observed in the absence of ABT-737 (right). **(b)** Fab AZ3 shows potent binding to BCL-xL in the presence of ABT-737 (left) and negligible binding was observed in the absence of ABT-737 (right).

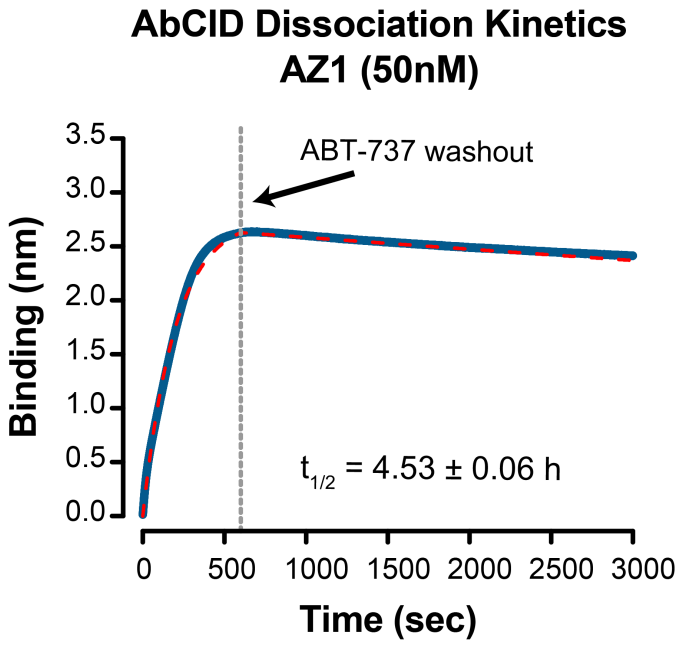

Supplementary Figure 5 Biolayer interferometry of Fab AZ1 with a washout of ABT-737. The blue curve represents measured data points and dashed red lines represents a local-fit line used for analysis. Fab AZ1 shows potent association to BCL-xL in the prescence of 1 μM ABT-737 and dissociation from the BCL-xL/ABT-737 complex upon washout of ABT-737. Data from one replicate is displayed and $t_{1/2}$ was calculated as a mean of 3 independent experiments ± s.d.

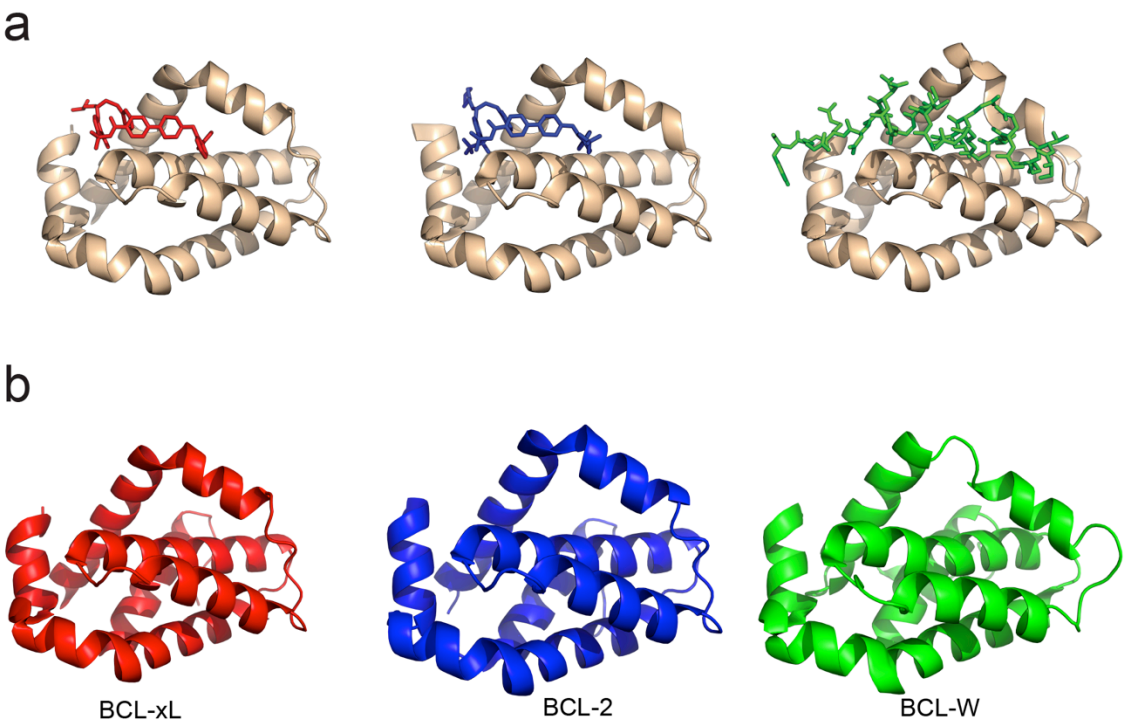

Supplementary Figure 6 Structures of BCL family proteins. **(a)** The crystal structures of ABT-737, ABT-263, and Bak-peptide bound to BCL-xL (PDB: 2YXJ, 4QNQ, and 5FMK) demonstrate that each ligand binds a nearly identical conformation of BCL-xL. **(b)** The crystal structures of BCL-xL, BCL-2, and BCL-W (PDB: 2YXJ, 4LVT, and 1O0L) show the similar fold and conformation of all three proteins.

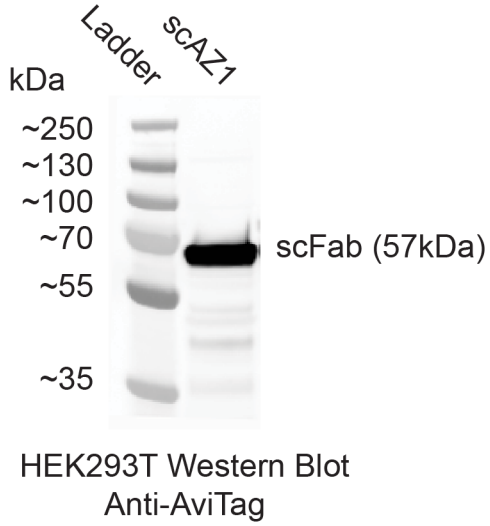

Supplementary Figure 7 Anti-AviTag immunoblotting of HEK293T cell lysate from cells transfected with *C*-terminal Avi-tagged scAZ1.

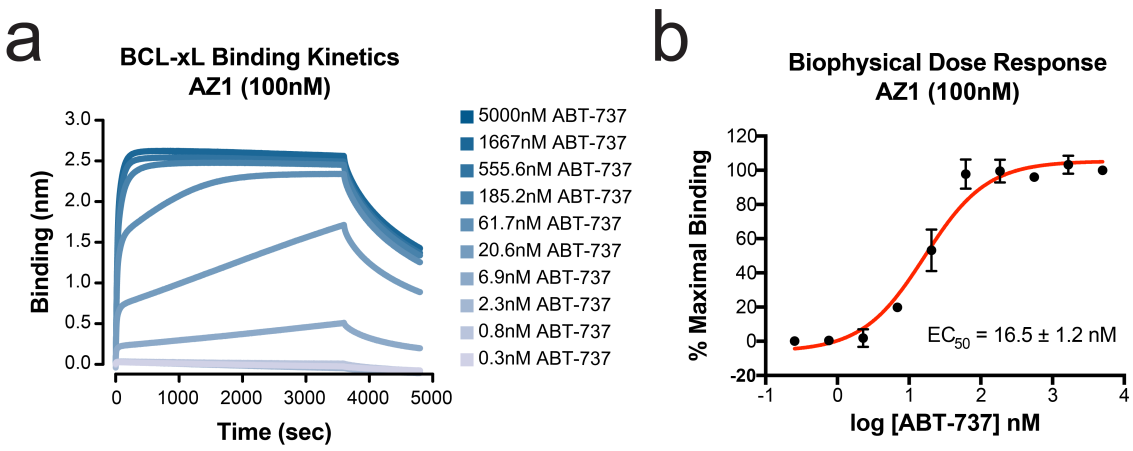

Supplementary Figure 8 Biolayer interferometry of Fab AZ1 with a titration of ABT-737. **(a)** Fab AZ1 shows ABT-737 dose-dependent binding to BCL-xL. (**b**) Dose-response curve for the induction of AZ1/BCL-xL dimerization by ABT-737. The binding (nm) signal for each ABT-737 concentration at 3600 s was normalized as a percentage of the signal for 5 µM ABT-737 at 3600 s. As saturated binding was not achieved at the lower concentrations of ABT-737 after 3600 s, the EC_{50} reported is likely higher than that which would be observed if the system were at equilibrium. Each data point represents the mean of 3 independent experiments ± s.d. The EC_{50} reported was calculated from the mean of 3 independent experiments using 3-parameter nonlinear regression ± s.e.m.

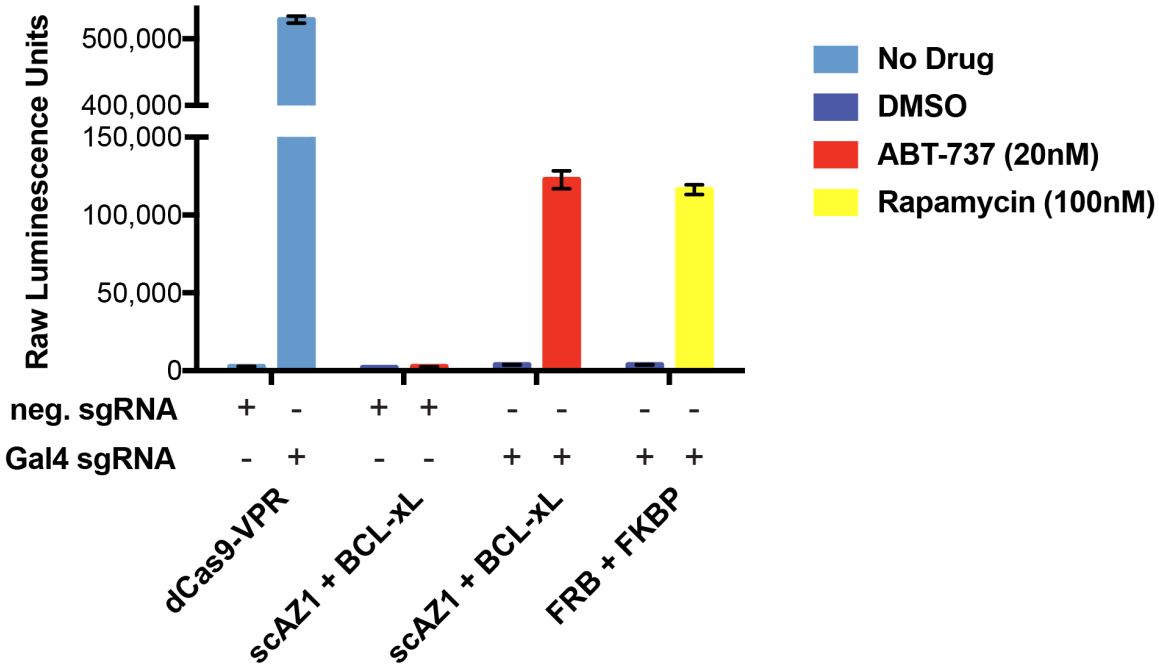

Supplementary Figure 9 Quantitation of luciferase activity 48 hours after addition of ABT-737 (20 nM) to the scAZ1 AbCID gene circuit or rapamycin (100 nM) to the conventional FKBP-FRB CID gene circuit. This raw data was used for normalization and generation of **Figure 3b**. Each data point represents the mean of 4 independent experiments ± s.d.

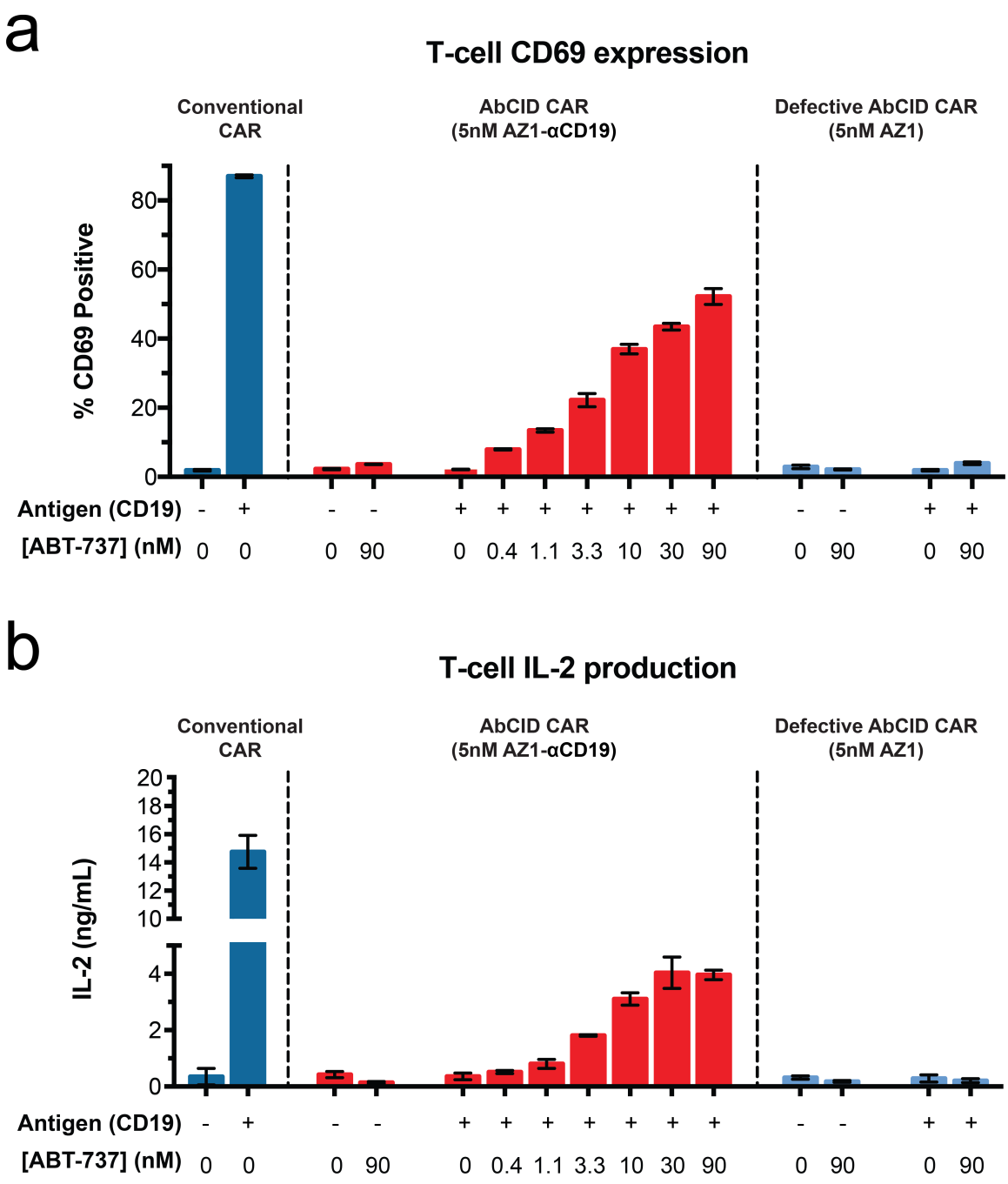

Supplementary Figure 10 Independent confirmation of CAR T-cell activation by the canonical markers CD69 and secreted IL-2 upon dose dependent AbCID activation. **(a)** Quantification of CD69 expression, as measured by immunofluorescence flow cytometry, 20 hours after initiation of co-culture with either $CD19^+$ or $CD19^-$ K562 target cells and addition of antibody (5 nM) and varying concentrations of small molecule. Addition of ABT-737 in the presence of $CD19^+$ K562 cells and bispecific antibody resulted in dose-dependent expression of CD69, but no expression was observed in the absence of ABT-737 or when co-cultured with $CD19^-$ K562 cells. The defective AbCID CAR, which lacks

the CD19-binding scFv portion of the antibody, elicited no expression of CD69 under all conditions. Each data point represents the mean of 3 independent experiments ± s.d. **(b)** Quantification of IL-2 secretion, as measured by ELISA, 20 hours after initiation of co-culture with either $CD19^+$ or $CD19^-$ K562 target cells and addition of antibody (5 nM) and varying concentrations of small molecule. Addition of ABT-737 in the presence of $CD19^+$ K562 cells and bispecific antibody resulted in dose-dependent secretion of IL-2, but no secretion was observed in the absence of ABT-737 or when co-cultured with $CD19^-$ K562 cells. The defective AbCID CAR, which lacks the CD19-binding scFv portion of the antibody, elicited no secretion of IL-2 under all conditions. Each data point represents the mean of 3 independent experiments ± s.d.

a

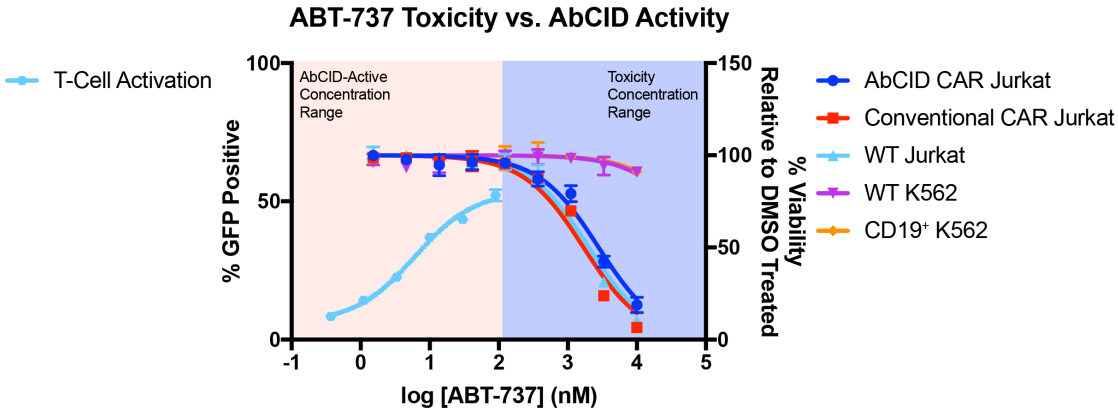

b

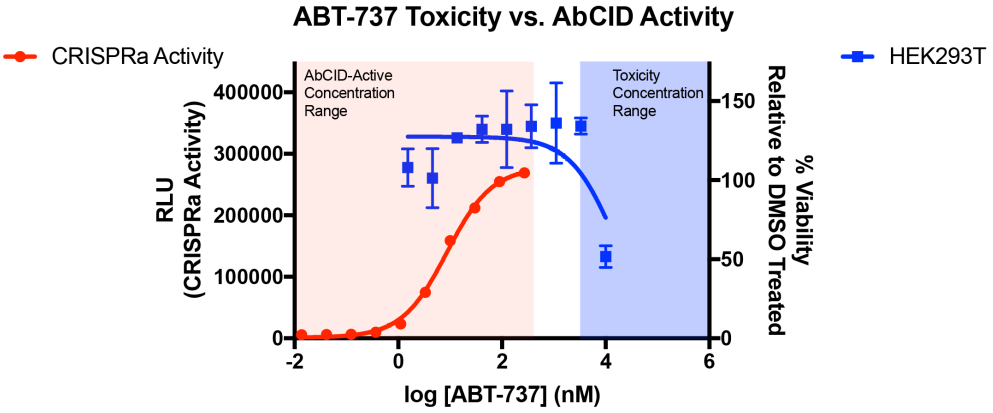

Supplementary Figure 11 The ABT-737 concentration range necessary for AbCID activation falls below that necessary for cell killing. **(a)** A CellTiter-Glo assay after 24 hours of ABT-737 treatment was used to measure the viability of Jurkat and K562 cells relative to DMSO treatment alone (right axis). Data is juxtaposed with CAR T-cell activation data from **Figure 4c** (left axis). The measured AbCID-activation concentration range was lower and exclusive from the toxicity concentration range. **(b)** A CellTiter-Glo assay after 24 hours of ABT-737 treatment was used to measure the viability of HEK293T cells relative to DMSO treatment alone (right axis). Data is juxtaposed with

luciferase activity data from **Figure 3c** (left axis). The measured AbCID-activation concentration range was lower and exclusive from the toxicity concentration range. Each data point represents the mean of 3 independent experiments ± s.d.

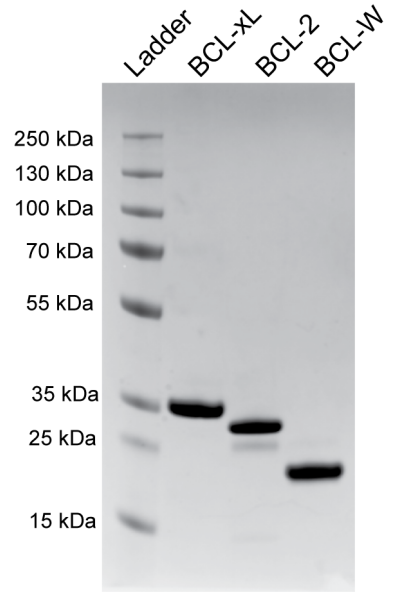

Supplementary Figure 12 SDS-PAGE analysis of the BCL-2 family members expressed and utilized as part of this study. 3 µg of each protein was diluted into loading buffer with reducing agent (BME).

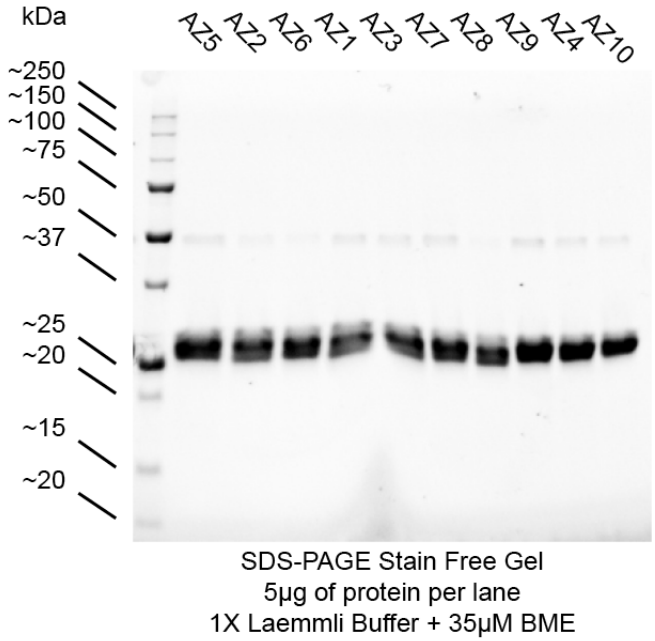

Supplementary Figure 13 SDS-PAGE analysis of the Fabs expressed and utilized in this study. 5 µg each of Fabs AZ1–10 were diluted in loading buffer with reducing agent (BME). Individual bands corresponding to the light and heavy chains can be seen.

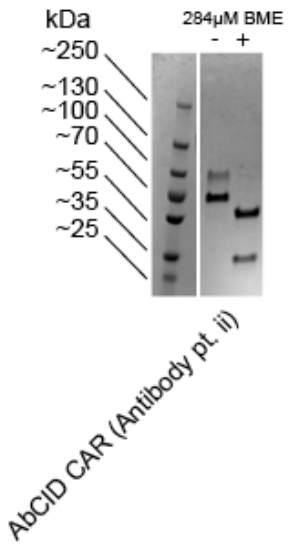

Supplementary Figure 14 SDS-PAGE analysis of the bispecific antibody expressed and utilized in this study. The bispecific antibody AZ1-αCD19 was diluted in loading buffer in the presence or absence of reducing agent (BME). Individual bands corresponding to the light and heavy chain can be seen in the presence of reducing agent.

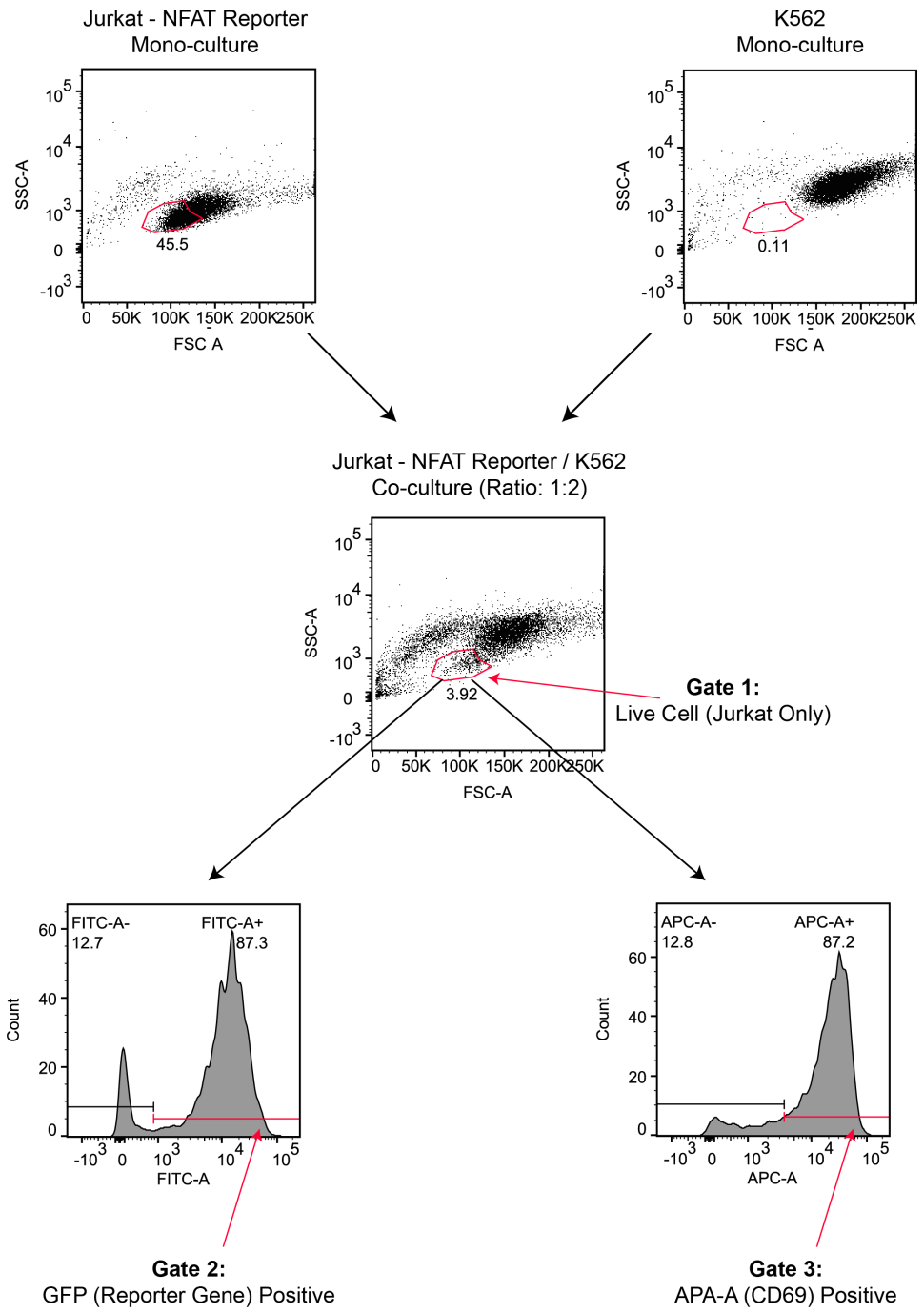

Supplementary Figure 15 CAR T-cell activation assay gating scheme. Jurkat - NFAT Reporter cells and K562s were assessed in isolation (Top) to determine a Live Cell (Jurkat Only) gate. For co-culture experiments, live Jurkat cells were gated (Gate 1), and GFP (Gate 2) and CD69 staining (Gate 3) positive populations were quantified.